



ORIGINAL ARTICLE

A Biofilm Channel Origin for Vermiform Microstructure in Carbonate Microbialites

¹School of the Environment, San Francisco State University, San Francisco, California, USA | ²Department of Geology, Bryn Mawr College, Bryn Mawr, Pennsylvania, USA | ³School of Life Sciences, University of Nevada, Las Vegas, Nevada, USA | ⁴Geological and Environmental Sciences, University of the Pacific, Stockton, California, USA | ⁵School of Geography, Earth and Environmental Sciences, University of Birmingham, Edgbaston, Birmingham, UK | ⁶Department of Earth Science, University of Southern California, Los Angeles, California, USA

Correspondence: Yadira Ibarra (yibarra@sfsu.edu)

Received: 17 May 2024 | Revised: 29 August 2024 | Accepted: 30 September 2024

Funding: This work was funded by the US National Science Foundation (NSF EAR 2038374 to Y.I., NSF EAR 2038420 to B.P.H., and NSF EAR 2038377 to L.K.R; P.J.M. by NSF award EAR 2221249).

Keywords: biofilms | carbonates | microbialites | microfossils | taphonomy

ABSTRACT

A three-dimensional tubular fabric known as "vermiform microstructure" in Phanerozoic and Neoproterozoic carbonate microbialites has been hypothesized to represent the body fossil of nonspicular keratose demosponges. If correct, this interpretation extends the sponge body fossil record and origin of animals to ~890 Ma. However, the veracity of the keratose sponge interpretation for vermiform microstructure remains in question, and the origin of the tubular fabric is enigmatic. Here we compare exceptionally well-preserved microbialite textures from the Upper Triassic to channel networks created by modern microbial biofilms. We demonstrate that anastomosing channel networks of similar size and geometries are produced by microbial biofilms in the absence of sponges, suggesting the origin for vermiform microstructure in ancient carbonates is not unique to sponges and perhaps best interpreted conservatively as likely microbial in origin. We present a taphonomic model of early biofilm lithification in seawater with anomalously high carbonate saturation necessary to preserve delicate microbial textures. This work has implications for the understanding of three-dimensional biofilm architecture that goes beyond the current micro-scale observations available from living biofilm experiments and suggests that biofilm channel networks have an extensive fossil record.

1 | Introduction

Characterization of morphologic attributes of fossilized organisms remains one of the most common methods of assigning taxonomic affinities to ancient and extinct organisms (Hopkins and Gerber 2017). However, taphonomic biases and morphologic similarities among fossil groups often complicate accurate taxonomic identification (Brasier, Antcliffe, and Callow 2011; Anderson et al. 2023). In instances when fossil or fossil-like remains contain parts resembling multiple taxonomic groups, assigning taxonomic affinities can be particularly challenging, especially for organisms whose body parts or community

structure lack symmetry, like sponges and microbial constructions (Mehra et al. 2020).

An anastomosing meshwork of microspar-filled tubules of varied diameter known as "vermiform microstructure," found in ancient microbialites and once considered microbial in origin (Walter 1972), has more recently been interpreted to represent keratose (nonspicular) sponges (Lee et al. 2014; Luo and Reitner 2014). This work has led to new reports of interpreted sponge body fossils in ancient carbonate microbialites, including vermiform microstructure in reefs from ~890 Ma (Turner 2021), thus potentially predating the oldest uncontroversial sponge

© 2024 John Wiley & Sons Ltd.

body fossils (Antcliffe, Callow, and Brasier 2014) by ~350 million years. The lack of scientific consensus on methodologies to distinguish between keratose sponge fossils and microbial textures remains problematic in their use to reconstruct past environments and reflect accurate evolutionary transitions (Kershaw, Li, and Li 2021; Neuweiler et al. 2023). Furthermore, recent experiments with extant microbial biofilms reveal similar vermiform geometries in the absence of sponges (Wilking et al. 2013; Zhang et al. 2018). Here, we use an exceptionally well-preserved microbialite from the rock record as a morphologic analog for a range of vermiform geometries increasingly attributed to keratose sponge body fossils and suggest an alternative interpretation for the origin and taphonomy of vermiform microstructure.

2 | The Cotham Marble as a Morphologic Analog for Vermiform Microstructure

The Upper Triassic Cotham Member of the Lilstock Formation of the southwestern United Kingdom contains laterally extensive stromatolitic and dendrolitic carbonate microbialite mounds (~20 cm thick, decimeters to meters in diameter) known as the Cotham Marble (CM) (Hamilton 1961; Wright and Mayall 1981). The CM microbialites were deposited in the shallow Tethys sea between Gondwana and Laurasia during a marine transgression on a shallow storm-dominated carbonate ramp that alternated between periods of restriction and connection to open marine waters (Hesselbo, Robinson, and Surlyk 2004). The CM coincides with the end-Triassic mass extinction interval (Ibarra et al. 2016) and led to the oldest nonskeletal marine seasonal temperature record (Petryshyn et al. 2020). Traceable laminated and dendrolitic phases of the CM across individual microbialite mounds indicate a strong environmental control on microscopic microbial features (Ibarra et al. 2015; Ibarra and Corsetti 2016). The microbialites are associated with an intermound, channel, flat-pebble conglomerate facies that formed from current reworking before lithification (Hamilton 1961).

Petrographic observations of the CM microbialites reveal vermiform geometries that are strikingly similar to the texture and fabric of vermiform microstructure from Phanerozoic and Neoproterozoic microbialites (Figure 1). Figure 1a compares the vermiform microstructure of Madiganites mawsoni (Figure 1a; Walter 1972) to textures in the first laminated layer (L1 in Ibarra et al. 2014) of the CM microbialites (Figure 1b,c). The bright, narrow, sinuous areas are composed of microsparitic calcite, while the darker regions are composed of micrite (Figure 1c). Figures 1d-killustrate similarities in texture between the CM and textures from the geologic record where the vermiform geometries are interpreted as the spongin network of keratose sponges. Basal stromatolitic laminations that comprise the lowermost laminated layer of the CM contain a tubular fabric (Figure 1d,e) that resembles the texture, size, and branching nature of vermiform geometries in Cambrian Cryptozoon stromatolites (compare Figure 1d to Figure 1f; Lee and Riding 2021) and in Upper Cambrian maze-like reefs (compare Figure 1e to Figure 1g; Lee et al. 2014). The tubular fabric is also present in the interdendrolite fill of the dendrolitic phases of the CM (Figure 1h) as well as within the dendrolites (see arrows in Figure 1i). Comparable tubular fabrics to Figure 1h,i of the CM have been described from Upper Ordovician micritic limestones (compare Figure 1h

to Figure 1j; Park et al. 2015) and Neoproterozoic reefs (compare Figure 1i to Figure 1k; Turner 2021). Given the petrographic similarities (Figure 1) between the tubular fabric in the CM and vermiform microstructures from the geologic record—interpreted as the permineralized spongin skeletal structure of keratose sponges (Lee et al. 2014; Luo and Reitner 2014; Park et al. 2015; Lee and Riding 2021)—we present a detailed description of the scales and variability of vermiform geometries in the CM and its associated facies (e.g., flat-pebble conglomerate) to provide clarity on the origin and taphonomy of seemingly identical enigmatic microstructures (Figure 1).

3 | Materials and Methods

3.1 | Ancient and Modern Geologic Samples

This work primarily focuses on detailed descriptions of petrographic fabrics containing different scales of vermiform geometries of Triassic CM samples from Bristol, Manor Farm, Stowey Quarry, and Lower Woods (see Appendix S1: Figure S1 for map of sites). We then compare the textures in the CM to similar geometries created in modern biofilms from the literature. Finally, we present a novel taphonomic model for the creation of vermiform microstructure using recent freshwater carbonates from the Spring Mountains of Nevada and examples from the geologic record (Ordovician mud mounds and microbialites of the Neoproterozoic Noonday Dolomite).

3.2 | Definition and Significance of Tubule Diameter

Vermiform microstructure is defined as a type of laminar architecture that consists of narrow, sinuous, pale-colored areas (usually sparry carbonate) surrounded by darker, usually fine-grained areas (usually micrite) (Walter 1972; Grey and Awramik 2020). In this text, we refer to the narrow, sinuous, sparry regions as "tubules" for their cylindrical morphology that, in many instances, displays round cross sections (Figure 1h), thus revealing their cylindrical (i.e., three-dimensional) morphology. Vermiform microstructure can be distinguished from similarly preserved "rectilinear" network fabrics composed of mostly criss-crossing straight lines of sparite with nodes interpreted as spiculate sponges (see figures 3 and 5 in Neuweiler et al. 2023). In this study, tubule diameter refers to the width of the sparry tubule. We note that the tubule diameter can vary slightly for a single tubule and thus use the terms "nearlyuniform" or "nearly consistent" diameter in reference to slight deviations from tubule uniformity.

While tubule diameter in the CM is variable, it is important to note that keratose spongin fibers—the rigid skeleton part of keratose sponges that has been attributed to vermiform microstructure—also exhibit diameter variability and size variability (Jesionowski et al. 2018; Stocchino et al. 2021). Nonetheless, the relative tubule uniformity between CM vermiform structures, biofilm channels (discussed in Section 5.2), and known sponge fossils is notable. Although tubule diameter is a criteria used to attribute vermiform microfabric to a sponge origin, it is not diagnostic, and other lines of evidence (such as macrostructure shape,



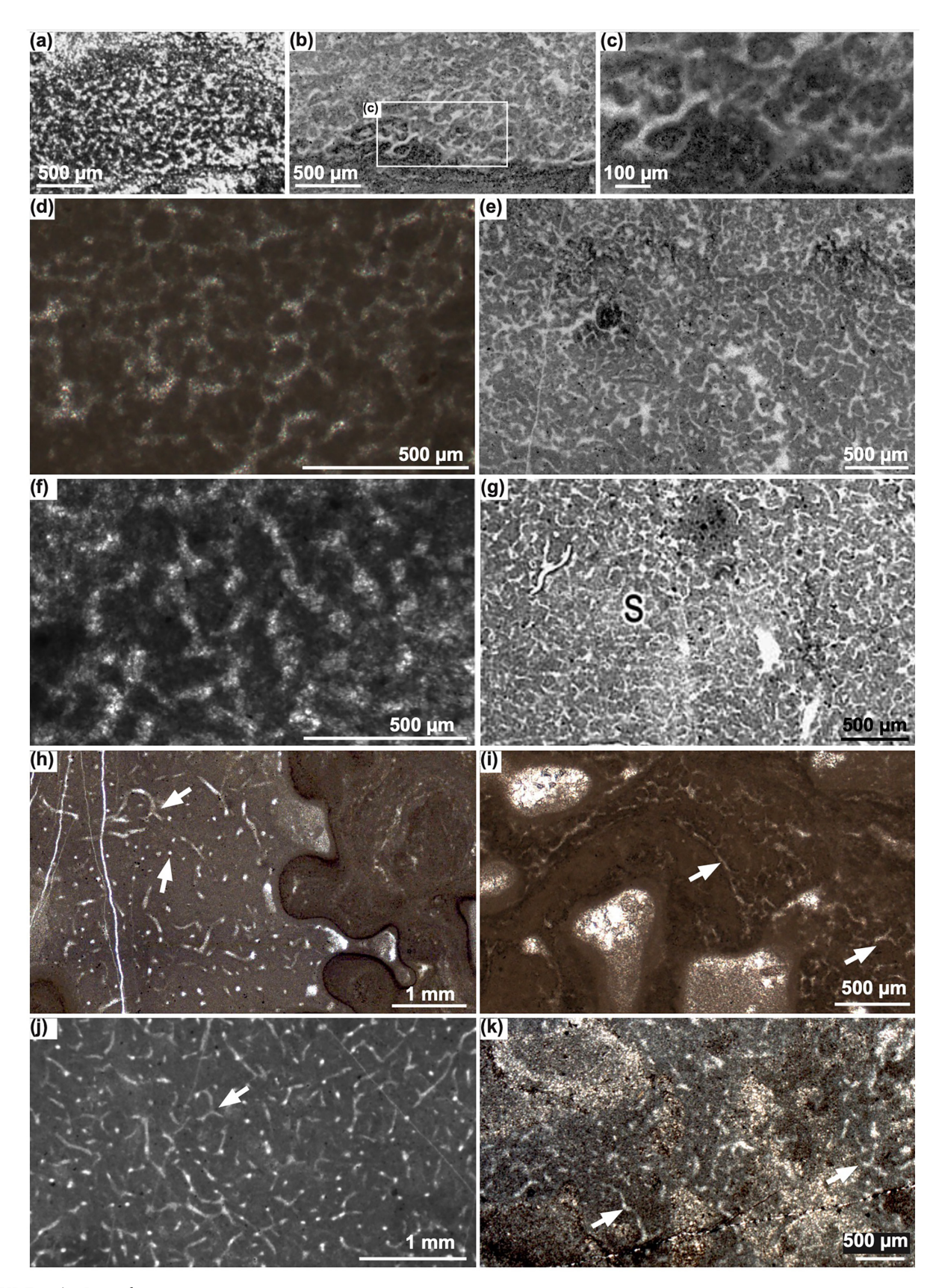


FIGURE 1 | Legend on next page.

tubule arrangement) must be used to ascertain biologic affinities (Luo et al. 2022; Neuweiler et al. 2023). In this text, we use

measurements of tubule diameters as a means of comparing to other reports of vermiform microstructure from the literature.



FIGURE 1 | Comparison of vermiform microstructure from the rock record to microstructures in the Cotham Marble microbialites. (a) *Madiganites mawsoni* from Walter (1972) considered a type of vermiform laminar architecture (Grey and Awramik 2020). (b) Bifurcating, microsparry, tubular geometries from the basal laminated layer (L1 in Ibarra et al. 2014) of the Cotham Marble microbialites. (c) Close-up of microspar-cemented microtubular fabric in a micritic matrix from the Cotham Marble. (d, e) Tubular microstructure from the basal laminated layer (L1) in samples from Bristol. (f) Vermiform geometries in Cambrian *Cryptozoon* stromatolites (Lee and Riding 2021); note resemblance in tubule size and geometry to (d). (g) Vermiform geometries in upper Cambrian maze-like reefs interpreted as a sponge ('S') texture (Lee et al. 2014); note resemblance in size and tubule microstructure texture and fabric to (e). (h, i) Microtubular structures in the dendrolitic phases of the Cotham Marble from Bristol (h) and Stowey Quarry (i) that occur in the interdendrolite region (h), and within the dendrolites (i). (j) Vermiform microstructure in upper Ordovician micritic limestones (Park et al. 2015) with arrow denoting similar branching morphologies to upper arrow in (h). (k) Vermiform microstructure from Neoproterozoic reefs (Turner 2021); compare to microstructure fabric, texture and size in (i) with tubules denoted with arrows.

3.3 | Tubule Diameter Measurements

Tubule diameter measurements were produced using image processing software (ImageJ; http://imagej.nih.gov/) (Appendix S1: Figures S2–S6, Tables S1–S3). Photomicrographs containing vermiform microstructure were binarized to highlight pixel intensity differences between dark (micritic) pixels and light (sparitic vermiform) pixels. The average tubule diameters were estimated using the Otsu thresholding method (Otsu 1979), which finds the optimal threshold based on the grayscale intensity values of the image pixels. The number of tubules and the minor axis of a best-fit ellipse for each tubule were quantified using the particle counting feature in ImageJ software with a particle size limit between $100\,\mu\text{m}^2$ and $10,000\,\mu\text{m}^2$.

4 | Results

4.1 | Description of Different Scales of Vermiform Microstructure in the CM Microbialites

The basal layer of the CM microbialites is comprised of micritic laminae (labeled "L1" in Ibarra et al. 2014). Vermiform fabrics occur along laminar bands ~5 mm thick (Figure 2a-c) and are microstratigraphically succeeded by fenestral fabrics typical of laminoid fenestrae (Tebbutt, Conley, and Boyd 1965; Choquette and Pray 1970; Figure 2d) and fenestral pores that form the axial zones of conical lamina (Ibarra et al. 2014; Figure 2e). The tubules display an anastomosing pattern (Figure 2f,g) and share similar microspar-filling cements with adjacent fenestral fabrics (compare Figure 2d,e,g). Measurements of tubule diameters in the CM resembling examples from the literature (e.g., Figure 1) are variable across all facies examined, with an average diameter of approximately $40 \mu m$ (36.5 ± 22 μm , n = 374; Figure S2, Table S1) and are composed of microspar separated by peloidal micritic aggregates that are ~50-100 µm in diameter (Figure 2c,f,g).

Dendrolitic layers of the CM microbialites (labeled "D1" and "D2" in Ibarra et al. 2014) exhibit remarkably evenly spaced (\sim 150 μ m in diameter) microbial branching patterns (Ibarra et al. 2014, 2015), resulting in interdendrolite spacing that is filled with sparry cement or micrite ("f" in Figure 3a). Bedding plane cross sections of the dendrolitic regions ("d") further highlight the bifurcating nature and diameter uniformity of the spacing between the dendrolite "branches" (Figure 3b). In other instances, oblique cross sections of polished slabs reveal the same branching tubular and semi-round cross sections of interdendrolite spaces with an average diameter of approximately

 $150\,\mu\mathrm{m}$ ($149.32\pm73.16\,\mu\mathrm{m}$, n=104; Figure 3c,d, Figures S3 and S4). These round to elliptical fenestrae are interpreted to result from early-lithified, evenly spaced, three-dimensional (3D) branching in microbial mats that result in round to elliptical voids when represented in two dimensions (Ibarra et al. 2014). High-resolution scans of the dendrolites reveal a network of submillimeter-scale branching tubules that prominently cap the upper regions of the dendrolites (Figure 3e–h). Detail of the internal structure of the dendrolites is shown in Figure 4, revealing the petrographic features of the network of branching tubules.

Many of the upper regions of the dendrolite branches are composed of what have been described as peloidal micritic fabrics (Ibarra et al. 2014), where the micritic aggregates are separated by microspar-filled anastomosing tubules (Figure 4b-d). While most dendrolites exhibit a laminated micritic texture (Ibarra et al. 2014), some are composed of peloidal micrite that is separated by an evenly spaced, microsparitic, tubular network (Figure 4). The tubules anastomose within the dendrolitic structures (Figure 4b-f) and strongly resemble the shape, size, and texture of vermiform geometries found in the basal laminated layers (Figure 2c). However, the preservation of the tubule structures is highly variable, such that some dendrolitic regions contain vermiform geometries where the tubules exhibit smaller-than-average diameters with distinct circular cross sections (~10 µm in diameter), somewhat resembling a 3D stitch pattern (Figure 4e,f). Micritic intradendrolite regions contain conspicuous pyrite-coated filamentous structures (black specs in Figure 4b) interpreted as possible microfossils whose pyrite composition was confirmed using a scanning electron microscope (SEM) coupled with energy dispersive spectroscopy (EDS) (Ibarra et al. 2014). Figure 4g summarizes the tubule diameter estimates for L1 and D1 facies of the CM microbialites and for the larger interdendrolite fenestra (Appendix S1: Figures S2, S3, and S4).

Vermiform geometries from the dendrolitic phases of the CM predominantly occur within the dendrolites, but there are rare examples where vermiform microstructures occur in micritic regions *between* the dendrolites (Figure 5). This interdendrolite micrite develops on and adjacent to the dendrolites (Figure 5b–d), suggesting a less-dense continuation of growth from the dendrolite structures, as is evidenced by the rounded protrusions that resemble the dendrolite morphology (Figure 5d) and the presence of bridging structures (*sensu* Marenco, Corsetti, and Bottjer 2002; Corsetti and Grotzinger 2005) that connect adjacent dendrolite "branches" (Figure 5b). Vermiform microstructures of variable geometries that display distinct circular cross



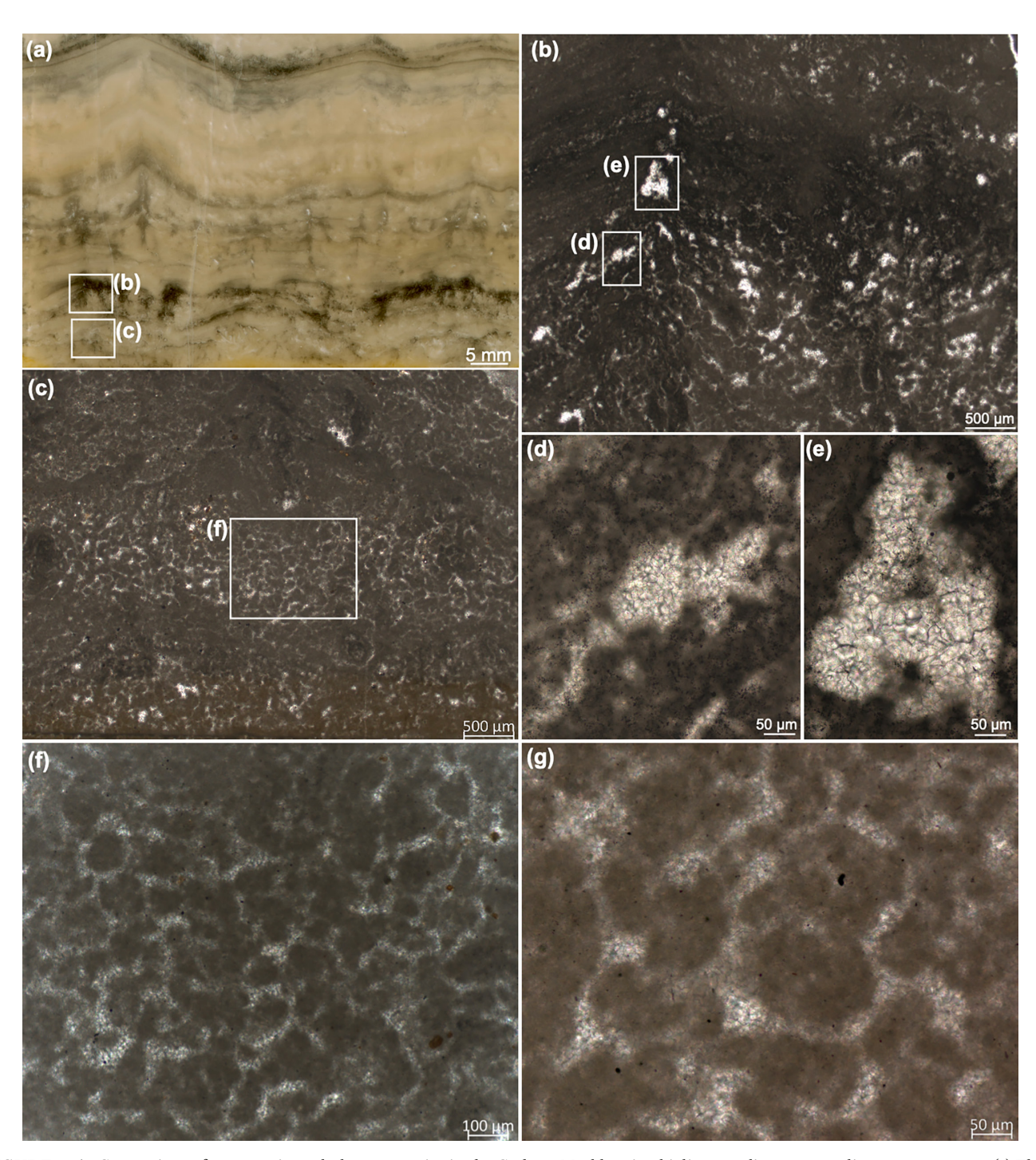


FIGURE 2 | Comparison of sparry microtubular geometries in the Cotham Marble microbialites to adjacent synsedimentary cements. (a) Thinsection, high-resolution scan of the laminated layer L1 from Bristol. (b) Micritic tuft and associated laminoid fenestra. (c) Vermiform microstructure. (d) Laminoid fenestra. (e) Fenestra associated with the tops of micritic tufted cones. (f) Close-up of vermiform microstructure in (c). (g) Detail of vermiform microstructure. Note the similarity in calcite cement fill between (d), (e), and (g) suggesting all were once open cavities that fill with synsedimentary cement.

sections (small arrows near the bottom of Figure 5d) occur in the interdendrolite micrite and are excluded from the microspar fill regions (Figure 5b–d). In a rare example, an isolated dendrolitic "branch" with a sharp linear boundary on one side was detected in the fill region (Figure 5e,f). The dendrolitic structure displays a well-preserved network of vermiform fabric as well as an internal larger (~150 μm diameter) ovoid cross section denoted by the central arrows (Figure 5f).

The CM microbialites are remarkably laterally extensive, whereby millimeter-scale features can be traced across their respective meter-scale mounds at different locations and up to ~100 km away from one another (Ibarra and Corsetti 2016). Here we demonstrate that the vermiform fabric associated with the dendrolitic phases can similarly be traced from site to site (Figure 6), suggesting an element of regional control on its development.



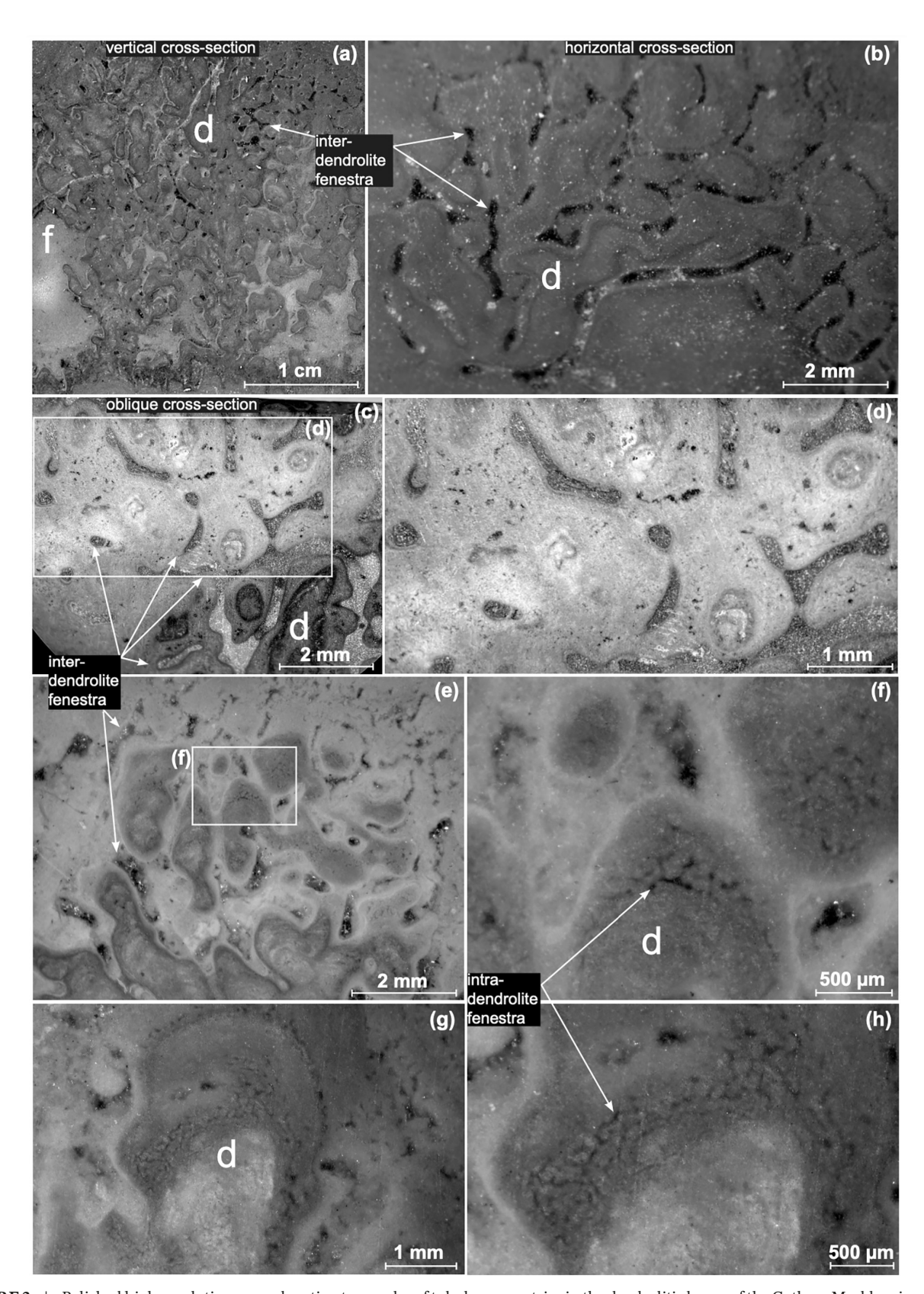


FIGURE 3 | Polished high-resolution scans denoting two scales of tubular geometries in the dendrolitic layers of the Cotham Marble microbialites. (a) Vertically oriented dendrolitic mesostructure (cm-scale) denoting the dendrolites "d" and interdendrolite regions "f." (b) Horizontal cross section of a polished sample through the dendrolitic region denoting the interdendrolite spacing of uniform diameter with arrows. (c, d) Oblique cross section of the dendrolites revealing interdendrolite regions with tubular branching and circular cross sections. (e–h) Mesostructure to microstructure detail of microtubular geometries labeled "intra-dendrolite fenestra" present within the dendrolites (arrows in f and h). Samples (a–d) are from Manor Farm and samples (e–h) are from Bristol.

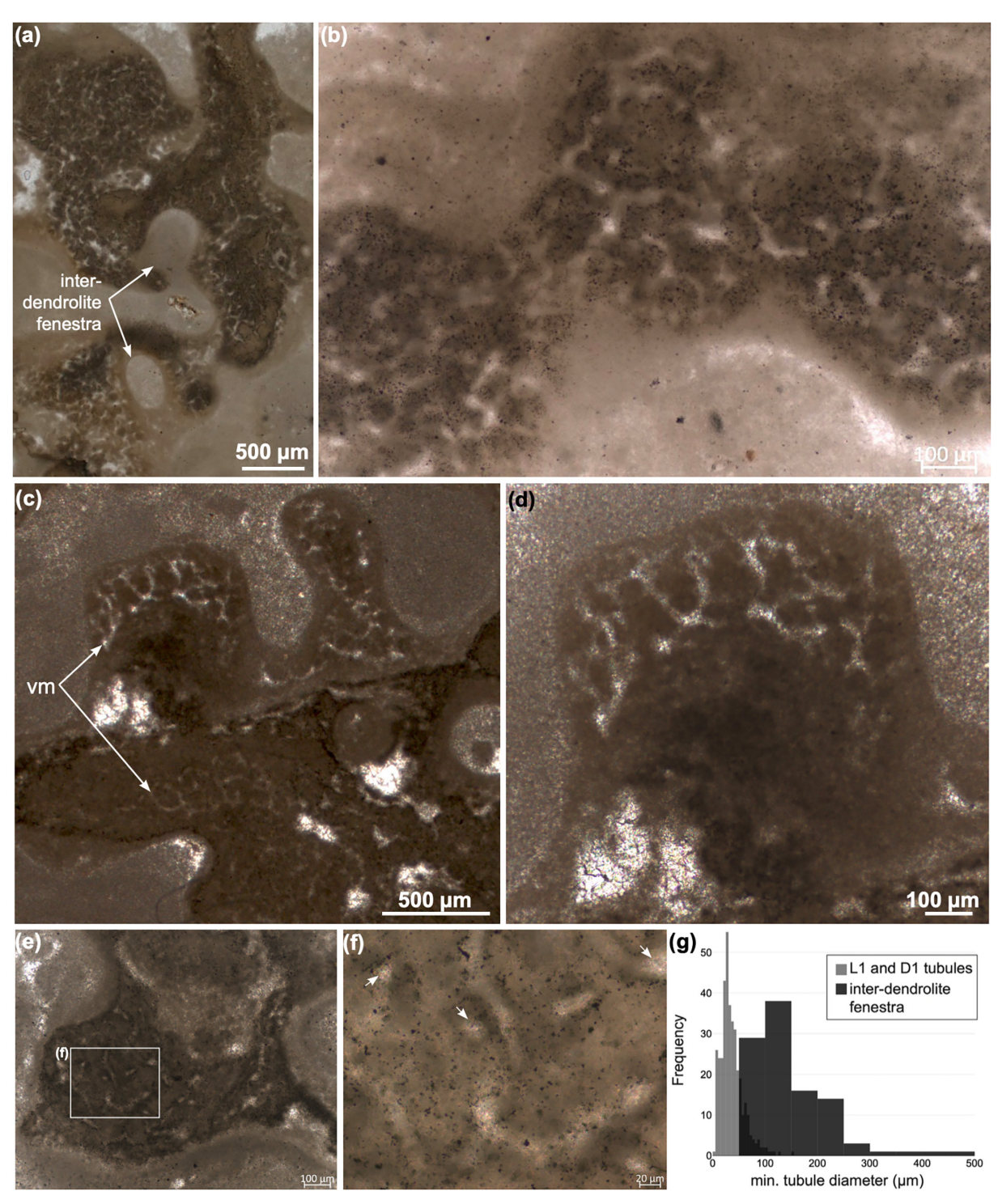


FIGURE 4 | Thin-section photomicrographs of intradendrolite vermiform microstructure in a sample from Stowey Quarry. (a) Submillimeter-scale branching morphology of a dendrolite. (b) Vermiform microstructures within the dendrolitic fabric are the bright, microsparitic tubular structures and the opaque dark features in the dark micritic regions are pyrite-coated possible microfossils (Ibarra et al. 2014). (c) Dendrolitic micritic protrusions that contain vermiform microstructure (vm) with anastomosing tubules of uniform diameter (d) higher resolution image of (c). (e, f) Vermiform geometries displaying somewhat of a 3D stitch pattern with distinct circular cross sections (arrows) in a micritic matrix that are restricted to the dendrolitic regions. (g) Histogram of minimum tubule diameters (in microns) measured for facies L1 and D1 of the CM microbialites and interdendrolite fenestra of CM microbialites (Appendix S1).

We also examined a flat-pebble conglomerate unit associated with the CM microbialites that resulted from current reworking in channels that separated the meter-scale mounds (Hamilton 1961). The low-sphericity flat-pebble clasts ("p") can

be up to ~8 cm long and are composed of fine-grained carbonate (Figure 7a-c). Previous studies demonstrated that some of the clasts act as nucleation surfaces for dendrolitic structures (Hamilton 1961). Indeed, petrographic analyses of flat-pebble



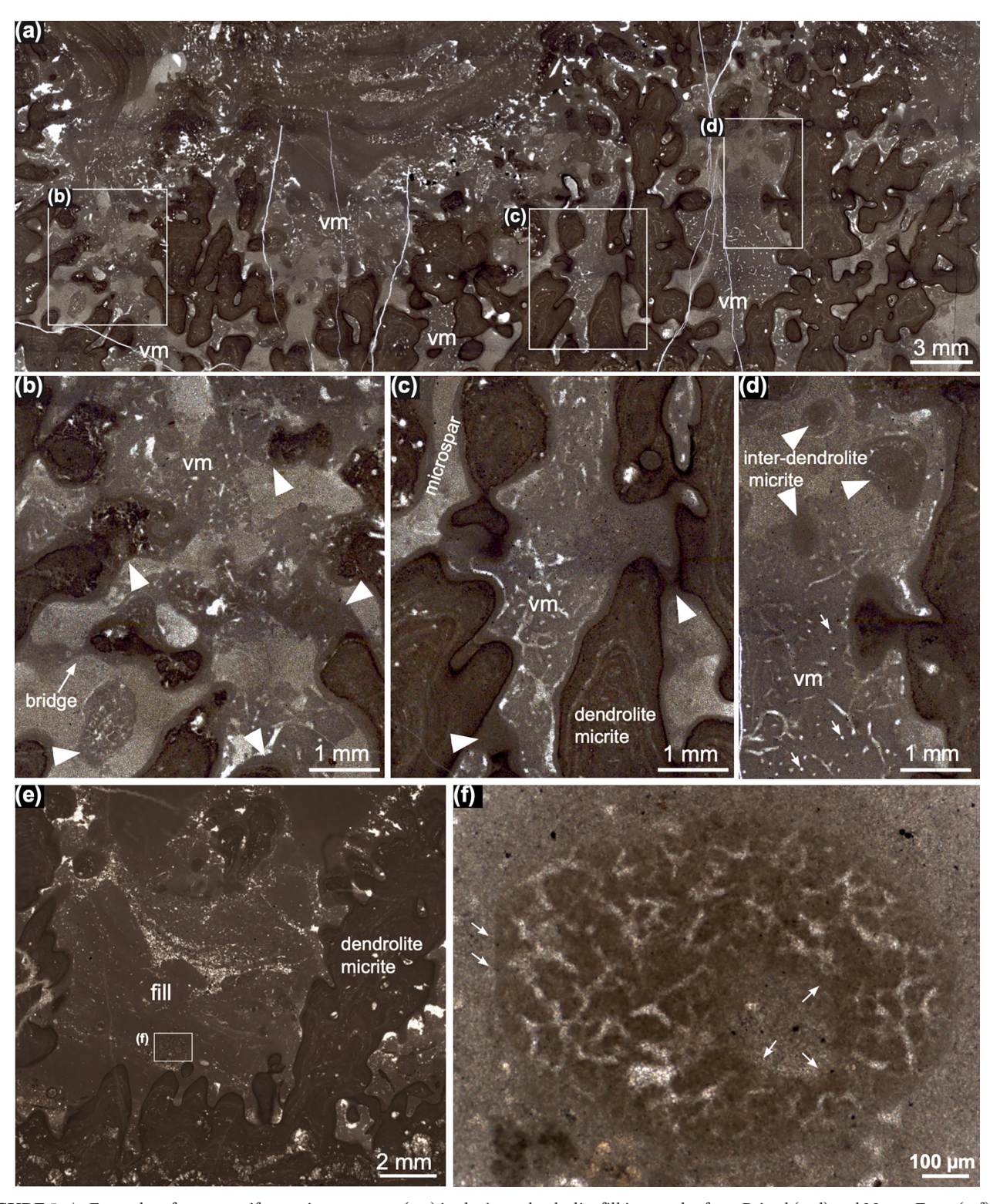


FIGURE 5 | Examples of rare vermiform microstructure (vm) in the inter-dendrolite fill in samples from Bristol (a–d) and Manor Farm (e, f). (a) Thin-section photomosaic of dendrolite phase D1 overlain by micritic laminae above. (b–d) Detail of (a) denoting with arrows the interdendrolite micrite and its associated vm; note the presence of a "bridge" structure (sensu Marenco, Corsetti, and Bottjer 2002; Corsetti and Grotzinger 2005) connecting adjacent dendrolite "branches" and clear circular tubule cross sections denoted with arrows in the lower part of (d). (e, f) A detached dendrolite "branch" deposited in the interdendrolite fill; the arrows in (f) denote a sharp boundary with the surrounding matrix and the arrows inside the dendrolite point to a larger-scale rounded morphology.

clasts reveal millimeter-scale micritic growths that develop on and, in some cases, form fringes around the pebble, somewhat resembling the dendrolitic phases of the CM in their micritic nature and domed morphology (see arrows in Figure 7a and protrusion petrographic detail in Figure 7b,c). The domical microdigitate protrusions have a semi-layered microstructure (Figure 7d), but



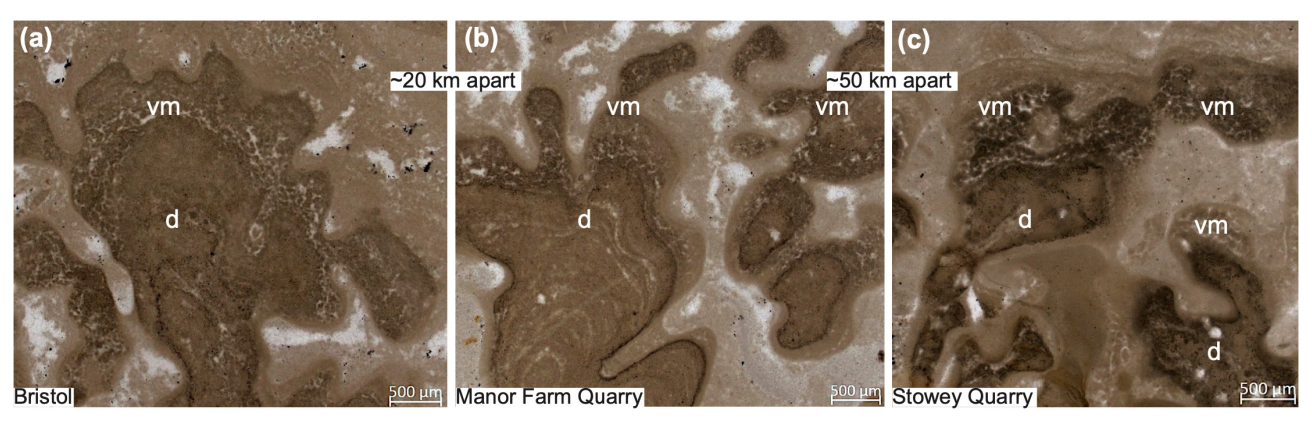


FIGURE 6 | Fine-scale lateral continuity of vermiform geometries across microbialite samples from three locations (a) Bristol, (b) Manor Farm Quarry, (c) Stowey Quarry, representing a minimum distance of at least ~20 km between sample sites (Ibarra et al. 2014; Ibarra and Corsetti 2016). All photomicrographs were taken using a white card; d = dendrolite; vm = vermiform microstructure.

are better classified as having a clotted (Shapiro 2000) micritic internal texture separated by microsparitic tubules that anastomose in the micritic framework, resembling the vermiform fabric described in the laminated and dendrolitic phases of the CM (Figures 2 and 4). In addition to the microsparitic bifurcating tubule structures (~40 μm in diameter), larger sparry features resembling the interdendrolite spacing (~150 μm in diameter) from Figure 3b,c are also present in the flat-pebble facies (arrows in Figure 7c).

5 | Discussion

5.1 | Assessing the Possibility of Sponges in the CM Microbialites

Here we have demonstrated that the CM microbialites contain a diverse array of vermiform geometries from dendrolite, stromatolite, interdendrolite regions, and flat-pebble conglomerate facies that are remarkably similar in size (~40 μm diameter), shape (tubular with round cross sections), branching nature (three-dimensional), and textural composition (microsparitic) to reported vermiform microstructures from the rock record, increasingly interpreted as the remnants of keratose sponge bodies. Below we consider observations from this study to evaluate the possibility that vermiform geometries of the CM represent sponge body fossils.

5.1.1 | Microfossil Distribution

It is well-known that microbes inhabit sponge tissues (Taylor et al. 2007), thus raising the possibility that the interpreted pyritic microfossils found in the micritic textures of the CM could be inhabitants of putative sponges. However, the pyritic fossil distribution is (1) restricted to micritic regions of the dendrolitic and laminated phases of the CM, and (2) does not scale to sponge morphologies (e.g., Botting 2005). In order for keratose sponges to be preserved through permineralization, at least somewhat of a mesoscopic body fossil should be produced that preserves the shape of the relic sponge (Neuweiler et al. 2023) as has been demonstrated for accepted examples of "sponge mummies" in lithistids (Froget 1976), hexactinellids (Brachert, Dullo,

and Stoffers 1987), and nonlithistid demosponges (Ritterbush et al. 2015). The distribution of pyrite filaments within the micritic regions (Figure 4; Ibarra et al. 2014), together with previously reported elevated total organic carbon (TOC) for the dendrolites versus the interdendrolite fill (Ibarra et al. 2014), indicates the pyrite structures are more likely microbial remnants associated with the creation and/or degradation of the dendrolitic and micritic regions (Ibarra et al. 2014), as opposed to lithified sponge tissue inhabitants.

5.1.2 | Lateral Continuity of mm-Scale Features

Vermiform microstructure has been shown to be laterally continuous for several meters, and its lateral continuity has been used as an argument against a possible sponge origin (Pratt 1982). Here we demonstrate the lateral persistence of vermiform microstructure across individual bioherms for samples collected up to ~50 km away from one another (Figure 6), suggesting a large-scale control on its development (sensu Ibarra and Corsetti 2016). While it is possible that sponges may have been responding to large-scale environmental forcings, it seems unlikely that some episodes of their development would (1) occur at precise "stratigraphic levels" up to ~50 km apart, (2) be limited to a thickness of ~0.5 mm (e.g., Figure 6), and (3) conform to the bounds of the preexisting dendritic morphology. On the cm-scale, the dendrolites of the CM are remarkably consistent in their dendrolitic habit (Ibarra et al. 2014), however, their microfabric is laminated or clotted (described here as vermiform) (Ibarra et al. 2014). If vermiform microstructure is indeed reflective of a sponge origin in the CM, then the creation of the dendrolites would be dependent upon the presence of spongin to give the dendrolites rigidity. The absence of vermiform microstructure in many dendrolites and the occurrence of vermiform microstructure at precise stratigraphic levels (Figure 6) implies it is not integral to the formation of the dendrolites or in giving them rigidity. Thus, a more parsimonious explanation for (1) the lateral continuity of mm-scale fabrics and (2) the presence and absence of vermiform microstructure in adjacent and within the same dendrolitic structure is that the dendrolites represent a microbial feature whose fabric (i.e., laminated versus vermiform) reflects a large-scale forcing.



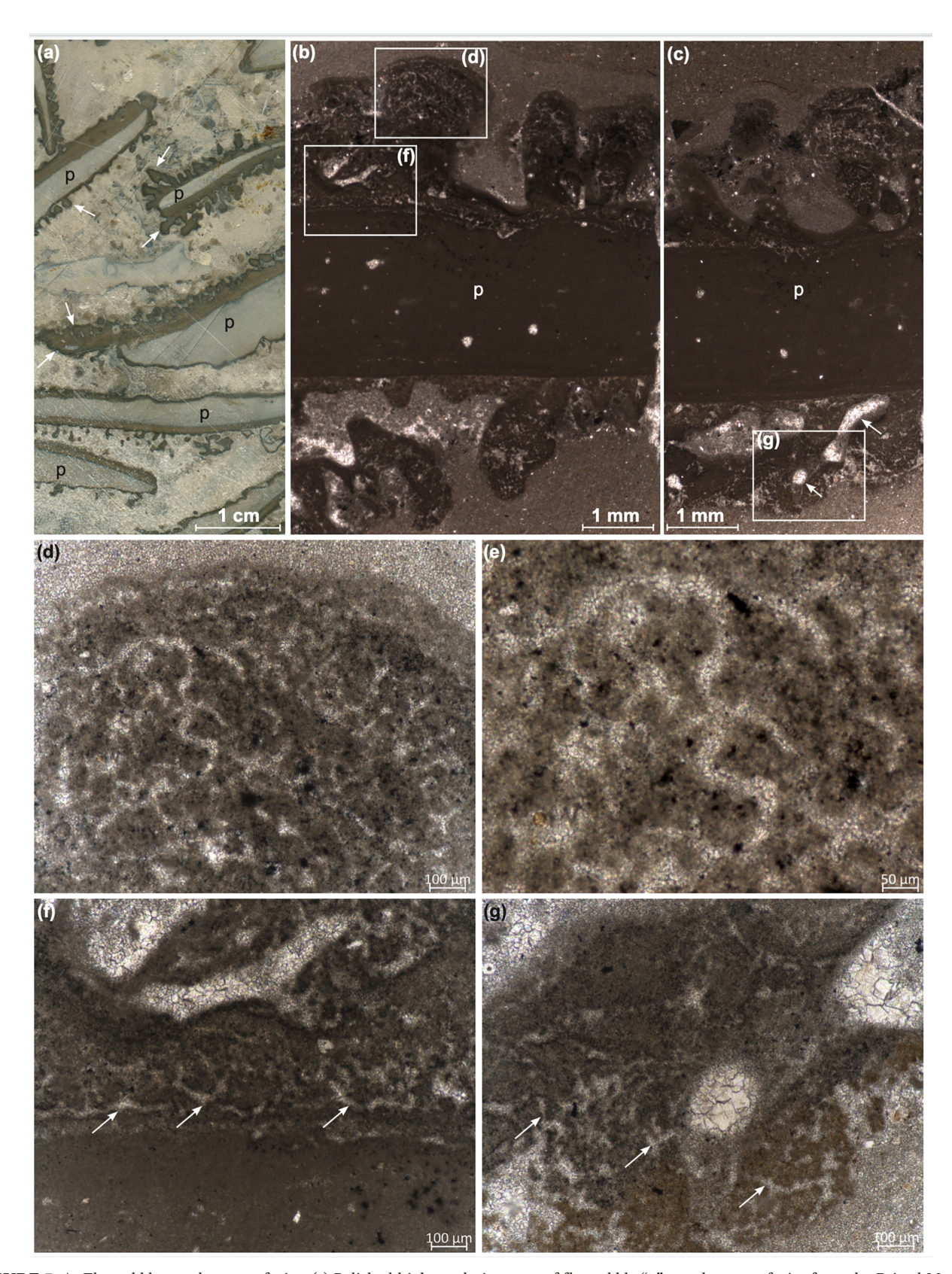


FIGURE 7 | Flat-pebble conglomerate facies. (a) Polished high-resolution scan of flat-pebble "p" conglomerate facies from the Bristol Museum and Art Gallery (labeled "Crazy" Cotham Marble, Specimen number CB 4144 B), arrows denote mm-scale micritic protrusions around the flat-pebble clasts. (b, c) Thin section photomicrograph cross section of a flat pebble "p" from Lower Woods showing millimeter-scale micritic protrusions, the arrows in (c) denote a larger-scale tubule structure similar to those labeled inter-dendrolite fenestra in Figure 3b–d. (d, e) Photomicrographs denoting detail in (b) that contain anastomosing, microsparitic tubular geometries separated by micritic regions. (f, g) Detail from (b) and (c) denoting with arrows the variable sparitic geometric patterns within the micritic protrusions.



5.1.3 | Vermiform Microstructure on Flat-Pebble Clasts

Thus far, most examples of vermiform microstructure have come from observations in microbialites or reefs from restricted lagoons to open shelf settings (Neuweiler et al. 2023), and here we show the occurrence of vermiform geometries of two different diameters (~40 µm and ~150 µm) in flat-pebble conglomerate facies representing shallow and possibly evaporative conditions (Hamilton 1961). Flat-pebble conglomerates are known to form after the seafloor has been partially lithified, and subsequent storm events or other high-energy conditions rip up the clasts and redeposit the lithified micrite (Sepkoski 1982). Flat-pebble clasts associated with the Cotham Marble are interpreted as intermicrobialite mound channel deposits that occasionally are found in the interdendrolite fill of the microbialites (Hamilton 1961). The fringing nature (Figure 7a) of the microdigitate structures implies they developed after the pebbles were ripped up and redeposited. The depositional setting (i.e., channel fill) and mm-scale morphology of the micrite (i.e., dendrolitic) suggest the micritic structures more likely represent the early development of microbial dendrolites like those of the CM, as opposed to lithified sponge bodies that colonized the fringes of flat-pebble clasts (Figure 7).

5.2 | A New Interpretation for Vermiform Microstructure: Lithified Biofilm Channels

A recent review of interpreted keratose spongin preservation in the rock record summarizes key caveats in the sponge interpretation for vermiform microstructure (Neuweiler et al. 2023). Most notably, there is no existing taphonomic pathway or model that can explain the permineralization of the spongin skeleton of a keratose sponge into microspar cement while also mummifying the sponge body and transforming it to homogenous fine-grained carbonate—all prior to compaction. While studies have questioned the spongin origin for vermiform microstructure (Kershaw, Li, and Li 2021), in the absence of a credible alternative hypothesis, the origin and taphonomy of vermiform microstructure remains an enigma. Below we propose a mechanism for the creation of vermiform microstructure that has yet to be considered in the vermiform microstructure debate, based on the diverse vermiform geometries and scale-dependent observations from the CM (centimetric to micro-metric), together with observations from the literature on modern biofilms and recent carbonate-coated grains.

5.2.1 | Biofilm Channels

Modern biofilm experiments demonstrate the creation of an anastomosing, tubular geometry by microbial biofilms in the form of intra-biofilm water channels (Lawrence et al. 1991; Costerton et al. 1994; de Beer et al. 1994; Stoodley, DeBeer, and Lewandowski 1994). In natural aquatic environments, surface-associated microbial communities are encased in a self-produced matrix of extracellular polymeric substances (EPS) that develop pores and interconnected channels (Lawrence et al. 1991; Flemming and Wingender 2010).

These nutrient-poor regions are also known as EPS matrix voids and represent water-filled regions in biofilms that exist between and within microbial clusters (Flemming and Wingender 2010). Biofilm channels can be distinguished from biofilm pores by their high length/width ratio (~> 10), whereas pores have length/width ratios that are closer to one (Quan et al. 2022).

Studies on modern biofilm cultures indicate channel formation is process-driven and that channels serve specific functions within biofilms such as particle transport and distribution of nutrients (Rooney et al. 2020). Wild-type *Bacillus subtilis* biofilms have been shown to produce highly interconnected, elongate channel networks (with an average channel diameter of $91\pm65\,\mu\text{m}$) that enhance the transport of liquids within biofilms (Wilking et al. 2013). The formation of channels in colonies of *Pseudomonas aeruginosa* is governed by biofilm growth rate and adhesion of the film to the substrate (Geisel, Secchi, and Vermant 2022). Channel networks in *Escherichia coli* biofilms indicate that intracolony channel morphologies are influenced by substrate composition and availability of nutrients (Bottura et al. 2022).

Most studies that have been successful in imaging the shape and structure of biofilm pores and interconnected water channels have done so on relatively thin biofilms, due to the technological limitations of imaging thicker, more mature, and hydrated biofilms (Yan et al. 2016). These procedural constraints restrict the opportunity for biofilms to create more complex 3D morphologies that may reveal the internal structural architecture of a mature biofilm. Similarly, field studies of living or recently lithified, mixed-community, aquatic biofilms that would be more representative of natural environments typically lose their architectural properties once removed from their in situ growth position.

The textures we describe in the CM are an example of an exceptionally well-preserved ancient microbialite that contains tubular fabrics that are similar in size, shape, and anastomosing nature to biofilm channels observed in microbial experiments (Figure 8a-c'). Reported channel diameters in extant microbial biofilms are within the range of tubule diameters found in vermiform microstructures from the CM (Figure 4g), but have highly variable widths (Lei et al. 2020; Bottura et al. 2022). Most imaging of biofilm channels has been on biofilm growth observed on flat surfaces (e.g., agar plates or microfluidic conduits), thus giving channels somewhat parabolic cross sections. As channels mature, they can develop circular cross sections (Wilking et al. 2013) similar to the round-cross sections observed in many examples of vermiform microstructure (Figures 1h and 4f).

5.2.2 | Three-Dimensional Tubular Aspect of Biofilm Channels

On a two-dimensional (i.e., flat) plane, modern biofilms create diverse geometries that resemble vermiform microstructure from the rock record (Figure 8a-c'). However, vermiform tubule architecture is three-dimensional in its branching nature (Luo and Reitner 2014), thus appearing to limit the applicability of their comparison to biofilm channels. In order for vermiform



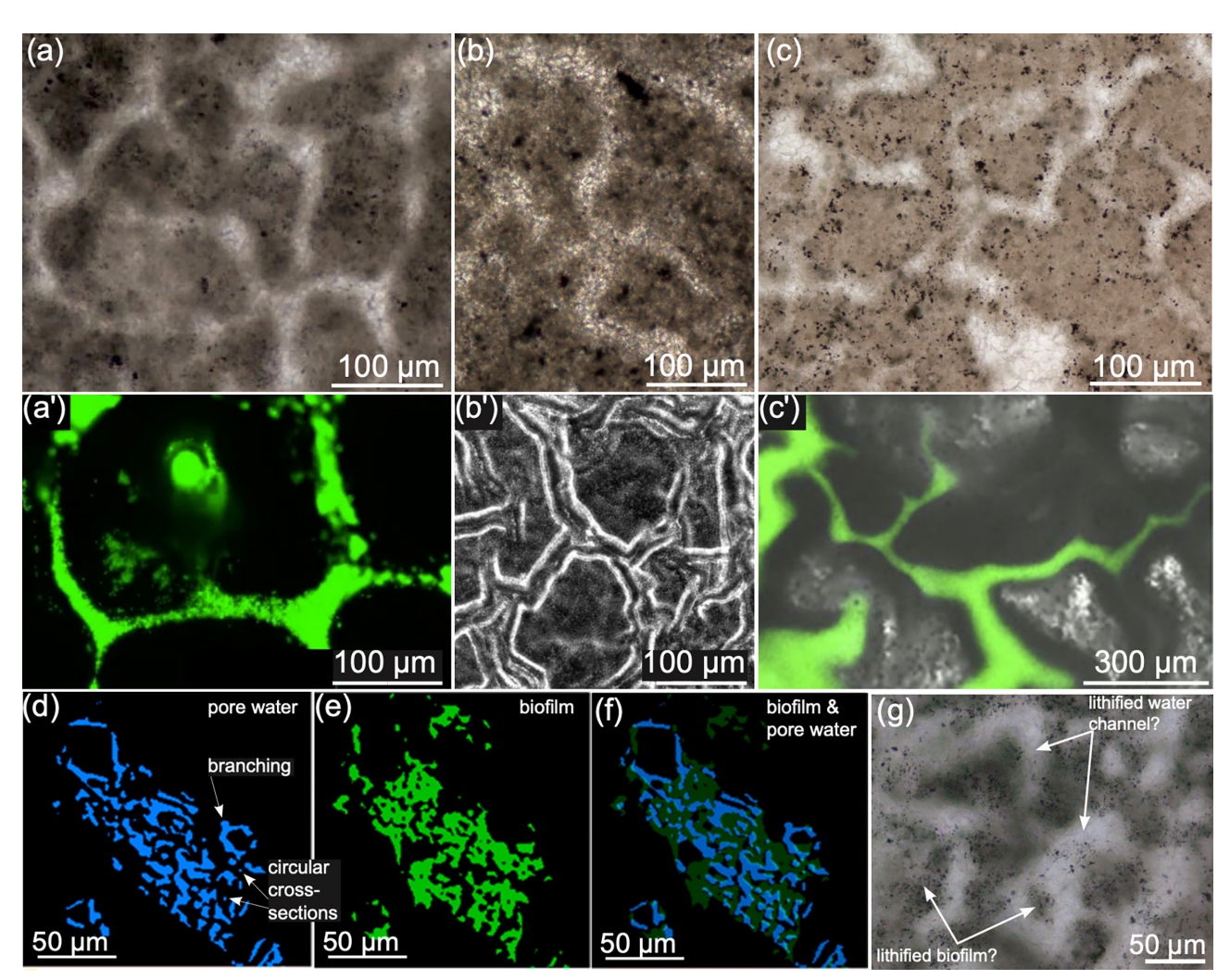


FIGURE 8 | Comparison of vermiform geometries to examples from modern biofilm channels. (a–c) Examples of tubular microstructure from the CM demonstrating similar morphologies to modern biofilm water channels (a') Wilking et al. (2013); (b') (Geisel, Secchi, and Vermant 2022); and (c') Wilking et al. 2013. Channel morphologies in (a') and (c') are highlighted with an aqueous fluorescent green dye imaged using confocal microscopy. (b') is a phase contrast image of a *Pseudomonas aeruginosa* biofilm where the development of hollow channels (pictured) are shown to increase the effective volume occupied by the biofilm (Geisel, Secchi, and Vermant 2022). (d–f) Pore water (d), biofilm (e), and (f) biofilm superimposed 2D relationships between the pore water and biofilm of a partitioned 3D biofilm sediment aggregate from Zhang et al. (2018). Note the tubular, branching geometries and circular cross sections of the pore water. (g) Interpretation of sparitic and micritic regions of the Cotham Marble as lithified water channels and biofilm.

microstructure to possibly represent lithified biofilm channels, modern biofilm water channels must show evidence for anastomosis in three dimensions that create a meshwork of tubules with somewhat uniform diameters that exhibit circular cross sections.

The 3D nature and tubular geometries of hydrated algal biofilm sediment aggregates (BSA) were recently observed using X-ray microcomputed tomography (μ -CT), which allows for the 3D visualization of fully hydrated biofilms without the need for desiccation (Zhang et al. 2018). The pore water component of the BSA is composed of 3D, tubular geometries that bifurcate and exhibit distinct circular cross sections that are enveloped by biofilm (Figure 8d–f; Zhang et al. 2018). The sizes of the tubular water channels in the BSA are smaller (~5–10 μ m in diameter)—yet still within the range of tubule diameters recorded in the CM (Figures 4g and 8g). While there is a slight difference in the tubule diameter size relative to the

size of vermiform microstructure from the rock record (~5–10 μm vs. ~40 μm), it is nonetheless intriguing that algal biofilms are able to create seemingly delicate water channels of nearly consistent diameter with complex, 3D branching, despite being enmeshed in detrital sediment, which could potentially smother the thin tubular structures.

Biofilms growing in carbonate environments and cavities with limited to no detrital and siliciclastic sedimentation are likely able to create increasingly complex water channel morphologies that exhibit near-isotropic anastomosis such as those shown in vermiform geometries of the CM. It has been shown, for example, that modern microbial mats reduce their morphological complexity during times of increased mud deposition (Mackey et al. 2017), and the majority of vermiform geometries reported from the rock record were deposited in carbonate environments with little to no detrital input (Neuweiler et al. 2023), potentially



allowing for the development of increasingly complex biofilm channel microstructures.

One advantage of being able to observe the larger, mesoscopic architecture of the dendrolites in the CM is that a larger-scale (~150 μm diameter), tubular architecture displaying anastomosis and circular cross sections is revealed (Figure 3b–d). These larger-scale interdendrolite fenestrae that emerge at the interface between dendrolite branches may represent a larger biofilm channel architecture that has yet to be described in modern laboratory-grown biofilms but is likely prevalent in natural aquatic substrates and possibly preserved in the geologic record under the right geochemical and environmental conditions.

5.3 | A Taphonomic Model for Vermiform Microstructure

The preservation of delicate tubular water channels within microbial biofilms necessitates a taphonomic model that accounts for the creation of two distinct textures (micrite and adjacent tubular microspar). We propose the micritic regions of vermiform geometries represent a micrite-precipitating community of microbes in a dense EPS matrix (Decho, Visscher, and Reid 2005; Dupraz and Visscher 2005; Dupraz et al. 2013), supported by the presence of possible microfossils (Figure 4; Ibarra et al. 2014), while the tubular bifurcating microspar represents the early (and likely syngenetic) precipitation of microspar cements within biofilm water channels or EPS-poor regions within the microbial structure (Figure 9a-c). In this model, the water channels transport and host supersaturated fluids with respect to calcite that ultimately precipitate sparry cements within them (Figure 9d), thus cementing and preserving the vermiform geometries (Figure 9e). Alternatively, scenarios may exist where the EPS portion of the biofilm becomes lithified, while the EPSpoor regions and water channels remain uncemented but preserved as porous tubular cavities (Figure 9c'). Upon return to supersaturated fluids, the tubular cavities can become cemented by pore-occluding sparry cements (Figure 9d).

Observations from Recent coated grains collected from cold spring carbonate environments in the Spring Mountains of Nevada show the creation of similar vermiform geometries preserved as tubular porosity along laminar bands of freshwater carbonate oncoids (Figure 10a-i). The texture created by the tubular shapes of the pores along the laminar bands of the oncoids is known as Spongiostromate in the microbialite literature (Flügel 2004) and is described as a very variable micritic, spongious, vermicular, fenestral, and peloidal texture (Gürich 1906). Spongiostromate oncoids were common in Proterozoic marine platform settings (Flügel 2004). Although the original description of Spongiostromate was used to describe a porous microbial texture (Gürich 1906), the resemblance of Spongiostromate microstructure to vermiform microstructure led to the recent sponge interpretation of the Mississippian Spongiostroma fossils (Lee and Riding 2022). In fact, observations from recent freshwater oncoids, which bear strong textural resemblance to their Proterozoic counterparts, reveal an important taphonomic step that is not always discernible in the study of ancient microbialites. The porous network present in the Recent oncoids from Figure 10 suggests that the creation of vermiform microstructure may involve a sequence of events that include (1) lithification of microbial EPS, followed by (2) the pore-occlusion of tubular cavities that may represent former intrabiofilm water channels or intrabiofilm EPS-poor regions (Figure 10). Estimates of tubule diameters do not show a statistically significant difference between L1 and D1 tubules in the CM microbialites and tubule pores in freshwater oncoids (Figure 10j, Figure S5), lending support for a similar origin for the tubule microstructures. In contrast, measurements of minimum tubule diameters for known spiculate sponges with a "sponge mummy" morphology and rectilinear sparitic microstructures reported in Neuweiler et al. (2023) show a statistically significant difference (p < 0.0001) to tubule diameter values in the CM microbialites (Figure S6, Table S3). The combination of (1) a sponge mummy mesostructure with (2) a distinct rectilinear sparitic microfabric and (3) larger tubule diameters than those typically reported for vermiform microstructure highlights important differences between accepted 'sponge mummies' (Neuweiler et al. 2023) and the observations presented herein for recent oncoids, the CM microbialites, and unlithified biofilm channels.

In the CM microbialites, it is unlikely that the microbialites experienced subaerial exposure that resulted in open cavities (Figure 9c') as in the Recent oncoid grains, but rather the microsparitic tubules were likely lithified nearly synchronously with the lithification of the biofilm under anomalously high carbonate supersaturation. Evidence for early lithification is demonstrated by the fully cemented vermiform network and surrounding micrite in what we interpret to be a microbial detachment structure (see figure 10 in Stewart 2012) that was sufficiently cemented in situ at the seafloor to maintain rigidity and preserve its microsparitic network together with its micritic rounded border and internal circular cross section of the larger scale (~150 µm) microbial branching (Figure 5e,f). The syngenetic precipitation of crystals in the biomass surrounding the tubular water channels is required for preservation of the two textures (micrite and microspar) in the CM microbialites. Studies have shown that EPS solutions produce smaller and more abundant CaCO₂ crystals compared to EPS-poor regions (Martinho De Brito et al. 2023), providing experimental context for the change in grain size from micrite to progressively more sparitic in the direction of a tubule or a pore. This taphonomic model of early cementation associated with carbonates that form in waters with anomalously high carbonate supersaturation or under evaporative conditions that lithify at or near the sediment water interface before compaction is well-recognized in the creation of fenestral fabrics (Choquette and Pray 1970).

Fenestra are defined as spaces that have no apparent support in the framework of primary grains composing the sediment (Tebbutt, Conley, and Boyd 1965), as is typical of vermiform microstructure. We consequently regard vermiform microstructure as a type of fenestral fabric (*sensu* Tebbutt, Conley, and Boyd 1965) representing a cement-filled primary void that is fabric selective. The highly variable vermiform geometries observed in the CM microbialites suggest that (1) there are likely intrinsic (e.g., microbial community composition) and extrinsic (e.g., environmental) controls on the creation of tubule geometries, (2) tubule preservation is largely dependent on the rates of calcification, and (3) not all features represent water channels



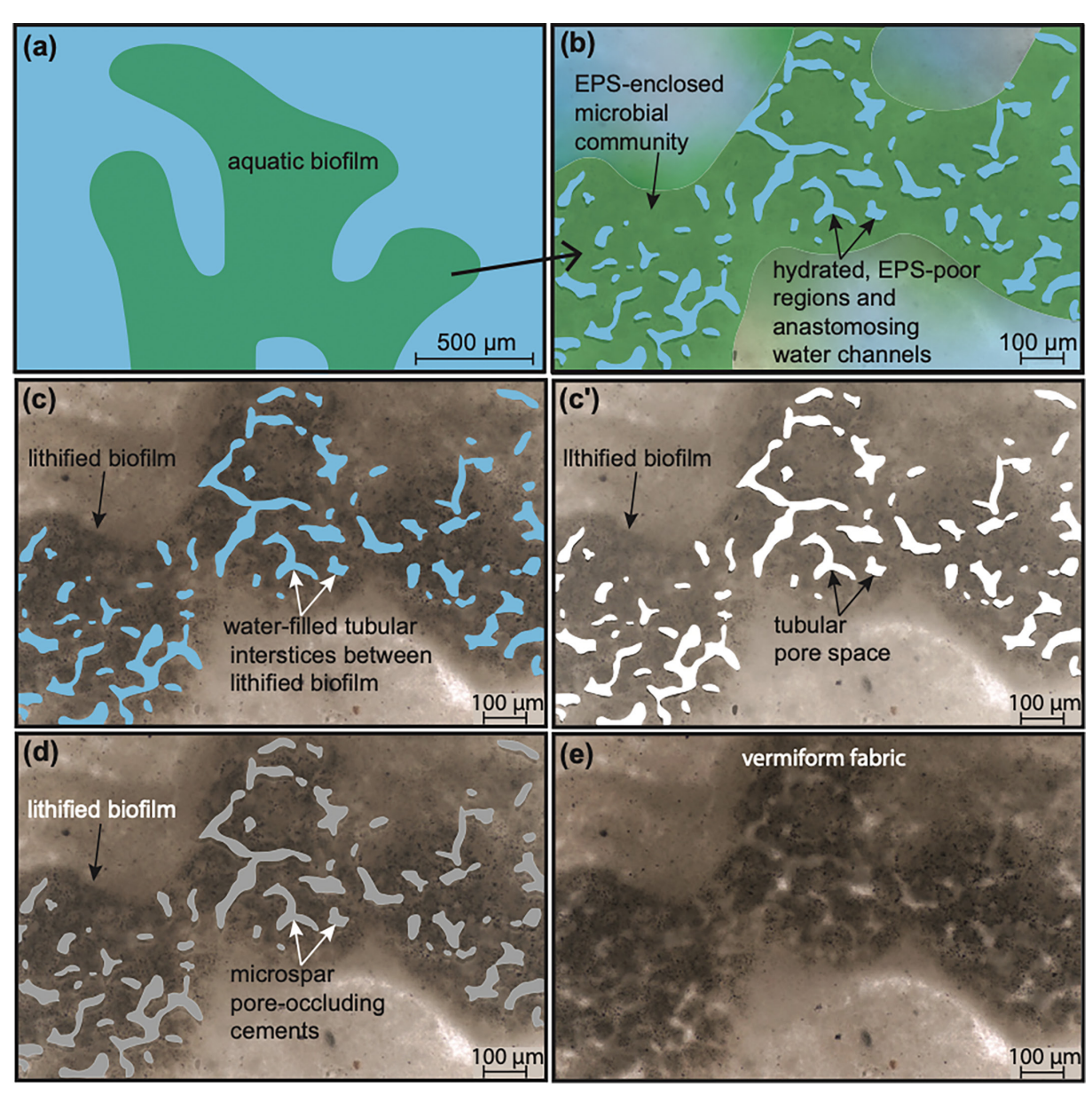


FIGURE 9 | A conceptual model of vermiform microstructure paragenesis. (a) Mesostructure of a living aquatic biofilm. (b) Detail of (a) where laminar and/or dendrolitic biofilms are composed of an EPS-enclosed microbial community with hydrated EPS-poor regions and anastomosing water channels. (c) EPS-rich regions of the biofilm are preferentially lithified by a micrite-precipitating microbial community leaving water filled, tubular interstices between the lithified micritic regions. (c') If the partially lithified biofilm is subaerially exposed, tubular pore space can result. (d) Microsparitic, pore-occluding cements fill the tubular interstices, creating a grain size contrast between the microsparitic tubules and the EPS-associated micrite. (e) Resulting vermiform microstructure.

sensu stricto but rather could simply represent EPS-poor or microbial-poor regions of the biofilm structure. While vermiform microstructure has been possibly attributed to fenestral fabrics (Neuweiler et al. 2023), the distinct, principal hypothesis of this study is the attribution of the tubular anastomosing geometries of variable morphologies that exhibit nearly uniform diameters (Figure 1) to biofilm channels described in modern experiments. The extreme diameter uniformity in tubule 3D architecture with distinct circular cross sections that typify some of the diagnostic examples of vermiform microstructure from the rock record (e.g., Park et al. 2015) likely represents an end-member of tubule morphology that is preserved under unique geochemical conditions. Deviations from diameter

uniformity and 3D branching likely represent biofilm pores or other microbial-poor regions of a biofilm.

The biofilm channel hypothesis for vermiform microstructure is further supported by additional observations in the CM microbialites. For example, the basal laminated layer of the CM contains evidence of restriction in the form of calcite pseudomorphs after gypsum (Ibarra et al. 2014), indicating evidence of hypersalinity. The occurrence of vermiform microstructure from shallow environments suggests the vermiform fabric could be a response to limited nutrient availability or a response to shallow water conditions. Biofilm channel formation increases permeability within hydrated biofilms (Costerton



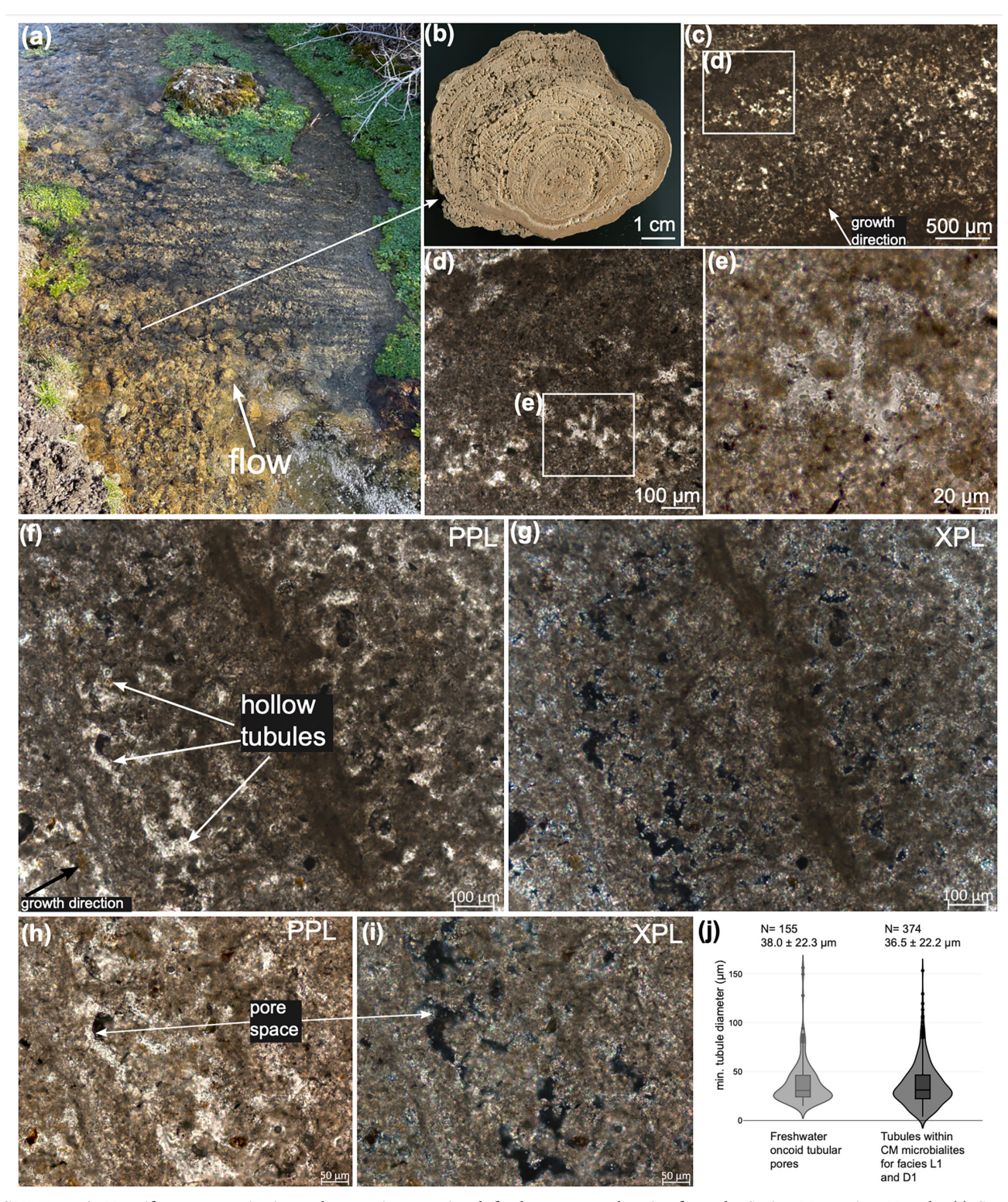


FIGURE 10 | Vermiform geometries in modern, spring-associated, freshwater coated grains from the Spring Mountains, Nevada. (a) Coated grains in an in situ position accrete along the creek. (b) High-resolution scan of a slabbed coated grain showing a well-laminated mesostructure. (c) Thin section photomicrograph of a laminar microstructure containing dense micritic bands that alternate with porous bands. (d, e) Detail of (c) showing a somewhat tubular open pore network in a micritic matrix. (f–i) Network of hollow tubules (arrows) aligned along laminar bands resembling vermiform geometries. (j) Violin plot showing similarity of tubular pore diameters in freshwater oncoids to L1 and D1 vermiform microstructure tubule diameters in CM microbialites. PPL, plane polarized light; XPL, cross-polarized light.

et al. 1994), suggesting that microtubule formation may represent a structural response for a need to increase water flow to the internal regions of a living biofilm, giving the tubules a

similar function to the vascular system of plants and animals (Penesyan et al. 2021). In turn, the delivery of seawater and solutes enhances the preservation potential of the channel's



(tubule) morphology via the delivery of carbonate ions that precipitate synsedimentary cements within them.

A remaining limitation in comparing non-lithified biofilms to microbialite rock textures is the uncertainty surrounding the effects of lithification on biofilm structural integrity. While biofilms can create 3D tubule networks (Figure 8), lithification of the biofilm must happen early enough (before burial) for the preservation of delicate tubule structures. Calcite precipitation within hollow tubule networks (e.g., Figure 9d) has yet to be demonstrated in a laboratory or natural setting, making it difficult to evaluate the extent to which pore-occluding cements may alter tubule morphology.

6 | Geologic Significance

Nearly all reported examples of vermiform microstructure attributed to keratose sponges occur within or are associated with microbialites—structures composed of lithified biofilms (Burne and Moore 1987)—thus lending support for a biofilm channel origin for vermiform microstructure. The biofilm channel hypothesis for the creation of vermiform microstructure based on experimental data can help explain several of its enigmatic features, including its (1) taphonomy, (2) temporal distribution, and (3) range of tubule diameters observed.

1. The uniform taphonomic mode of preservation for vermiform fabric (i.e., microsparitic tubules in a matrix of micrite) likely results from the cementation of open biofilm channels (tubules) after lithification of the EPS portion of the biofilm, which is a similar process to the precipitation of synsedimentary cements that fill fenestral textures (Figure 2d,e). Similarly delicate metabolic gas bubbles within biofilms have been shown to leave a morphologic record in ancient stromatolites and are often preserved as microspar-filled fenestrae (Bosak et al. 2009). While bubble formation is a distinct process from the hypothesized creation of tubular channels described herein, bubbles are also seemingly delicate structures that are preserved nonetheless under the right geochemical conditions. It is likely that water-filled anastomosing channels observed in modern biofilms can preserve a morphologic record of tubular geometries if the microbial community develops in aquatic environments

- with anomalously high supersaturation with respect to calcium carbonate to promote rapid lithification.
- 2. Accordingly, there is a preponderance of vermiform microstructure reports in microbialites that formed during times of anomalously high seawater carbonate saturation. These time periods include, but are not limited to, the Neoproterozoic (Turner 2021), the Cambro-Ordovician (Lee and Riding 2021), the Cambrian (Lee et al. 2014), the Triassic (Pei et al. 2021; Wu et al. 2022), and the aftermath of the end-Permian (Heindel et al. 2018; Baud et al. 2021), providing a temporal and geochemical mechanism for the preservation of delicate biofilm microstructures. Many of the examples listed also occur adjacent to and in the interstices of calcium carbonate crystal fans (Friesenbichler et al. 2018; Baud et al. 2021), which represent hallmarks of anomalously high carbonate supersaturation (Grotzinger and Knoll 1995; Woods et al. 1999). Thus far, channel networks and lithified biofilm microstructures have been attributed to micritic veneers lining carbonates from cryptic habitats (Riding 2002), and here we suggest that lithified biofilm channel networks may be more common than previously considered.
- 3. The interpretation of vermiform fabric as biofilm channels also addresses the range of microtubule sizes observed for vermiform geometries from the same rock unit or within a single microbialite unit (Luo and Reitner 2016; Friesenbichler et al. 2018). Modern microbial mats exhibit network fabrics that occur at many scales, resulting in fractal-like morphologies (Kropp et al. 1997). Similar larger geometries of 3D microstructures can be found in modern microbial mats (Shepard and Sumner 2010; Sim et al. 2012), resulting from microbial mat growth in systems limited by diffusion (Petroff et al. 2010). In the CM microbialites, we observe at least two microstructural scales of fenestra development associated with the dendrolitic layers (inter- and intradendrolite spacing labeled in Figure 3). Many of the dendrolite structures also exhibit classic mushroom shapes in vertical cross section (Figures 4c,d and 7b), which represent the observed and modeled architecture of a mature biofilm macrocolony (Flemming and Wingender 2010). Recent interpretations of larger round morphologies associated with vermiform microstructure have been attributed to sponge canals (Lee and Riding 2022; Luo et al. 2022), but can be more parsimoniously explained by a larger scale of biofilm

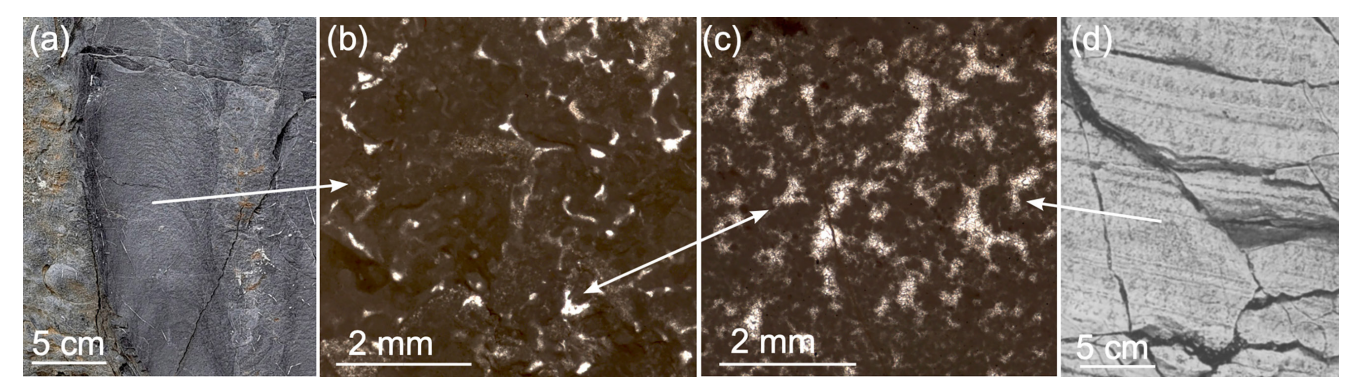


FIGURE 11 | Larger-scale fenestral patterns in microbialites from the rock record. (a) Stromatolitic reefs from the Ordovician denoting with arrows the larger-scale fenestral pattens in a thin-section photomicrograph (b). (c) Noonday Dolomite photomicrograph of micritic shrub facies (c) and outcrop photo (d) from (Fraiser and Corsetti 2003) with comparison to larger-scale fenestral patterns to (b).



fenestrae, demonstrated in the CM as interdendrolite spacing (Figure 3). The shape and size of the larger tubular features would help explain the range of vermiform diameters seen in microbialite deposits (Luo and Reitner 2014, 2016; Lee and Riding 2022). Similar fractal-like fenestral patterns are common in other ancient microbialites such as Ordovician stromatolitic reefs (Figure 11a,b), the Neoproterozoic Noonday Dolomite (Fraiser and Corsetti 2003) (Figure 11c,d), as well as in modern dendrolitic cones in hot spring settings (Bradley et al. 2017).

The similarity in shape, size, and distribution of microspar-filled tubules in a micritic matrix within a microbialite unit shared with channel geometries in extant microbial biofilms indicates that vermiform microstructure can be created in the absence of sponges. Microbial communities produce 3D channel networks that could potentially be preserved in the geologic record as anastomosing tubular microstructures. If the biofilm channel hypothesis for vermiform microstructure is correct, it would allow for a unique understanding of mature 3D biofilm architecture that extends to at least the Neoproterozoic (Turner 2021), which is often difficult to resolve in modern biofilm analyses (Yan et al. 2016). As sampling and imaging techniques on living natural aquatic biofilms improve, modern observations will help reveal the significance of the variable vermiform geometries observed in the rock record. We do not suggest that all reports of sponge body fossils that contain a tubular texture represent microbial features. For example, exceptionally preserved chitin in a sponge fossil from the Burgess Shale preserves features attributed to a keratosan sponge that scales with the shape of the skeletal sponge body fossil (Walcott 1920; Ehrlich et al. 2013). Instead, our analyses provide sufficient evidence for a need to reevaluate the keratose sponge interpretation for vermiform microstructure in carbonate microbialites and in turn may reveal a new opportunity to explore the significance of biofilm channel networks at different scales of biofilm development in ancient carbonates.

7 | Conclusion

We describe a wide array of vermiform geometries in the Upper Triassic Cotham Marble microbialites. The vermiform geometries are comparable and nearly identical to many examples of vermiform geometries from Phanerozoic and Neoproterozoic microbialites that have been interpreted as keratose sponge body fossils. Observations of microfossil distribution, lateral continuity, and flat-pebble facies are all evidence against the presence of sponges in the CM microbialites. Comparison of modern biofilm channels with vermiform geometries in the CM microbialites and recent freshwater oncoids suggest a similar origin. We hypothesize that vermiform microstructure is a morphologic record of cemented intrabiofilm water channels in ancient microbial deposits that grew in seawater with anomalously high carbonate supersaturation.

Acknowledgments

We thank Patrick Browning and Connor Penrod for field assistance and access support in the Springs Mountains Nevada under permit number

SMA0463. Financial support was provided by NSF EAR 2038374 to Y.I., NSF EAR 2038420 to B.P.H., and NSF EAR 2038377 to L.K.R. P.J.M. was supported by NSF award EAR 2221249.

Conflicts of Interest

The authors declare no conflicts of interest.

Data Availability Statement

The data that supports the findings of this study are available in Appendix S1 of this article.

References

Anderson, R. P., C. R. Woltz, N. J. Tosca, S. M. Porter, and D. E. G. Briggs. 2023. "Fossilisation Processes and Our Reading of Animal Antiquity." *Trends in Ecology & Evolution* 38: 1060–1071.

Antcliffe, J. B., R. H. T. Callow, and M. D. Brasier. 2014. "Giving the Early Fossil Record of Sponges a Squeeze." *Biological Reviews* 89: 972–1004.

Baud, A., S. Richoz, R. Brandner, et al. 2021. "Sponge Takeover From End-Permian Mass Extinction to Early Induan Time: Records in Central Iran Microbial Buildups." *Frontiers in Earth Science* 9: 1–23.

de Beer, D., P. Stoodley, F. Roe, and Z. Lewandowski. 1994. "Effects of Biofilm Structures on Oxygen Distribution and Mass Transport." *Biotechnology and Bioengineering* 43: 1131–1138.

Bosak, T., B. Liang, S. S. Min, and A. P. Petroff. 2009. "Morphological Record of Oxygenic Photosynthesis in Conical Stromatolites." *Proceedings of the National Academy of Sciences of the United States of America* 106: 10939–10943.

Botting, J. P. 2005. "Exceptionally Well-Preserved Middle Ordovician Sponges From the Llandegley Rocks lagerstätte, Wales." *Palaeontology* 48: 577–617.

Bottura, B., L. M. Rooney, P. A. Hoskisson, and G. McConnell. 2022. "Intra-Colony Channel Morphology in *Escherichia coli* Biofilms is Governed by Nutrient Availability and Substrate Stiffness." *Biofilms* 4: 1–14.

Brachert, T. C., W.-C. Dullo, and P. Stoffers. 1987. "Diagenesis of Siliceous Sponge Limestones From the Pleistocene of the Tyrrhenian Sea (Mediterranean Sea)." *Facies* 17: 41–49.

Bradley, J. A., L. K. Daille, C. B. Trivedi, et al. 2017. "Carbonate-Rich Dendrolitic Cones: Insights Into a Modern Analog for Incipient Microbialite Formation, Little Hot Creek, Long Valley Caldera, California." *NPJ Biofilms and Microbiomes* 3: 32.

Brasier, M. D., J. B. Antcliffe, and R. H. T. Callow. 2011. "Evolutionary Trends in Remarkable Fossil Preservation Across the Ediacaran-Cambrian Transition and the Impact of Metazoan Mixing." In *Taphonomy: Process and Bias Through Time*, edited by P. A. Allison and D. J. Bottjer. Dordrecht, the Netherlands: Springer.

Burne, R. V., and L. S. Moore. 1987. "Microbialites: Organosedimentary Deposits of Benthic Microbial Communities." *PALAIOS* 2: 241.

Choquette, P., and L. Pray. 1970. "Geologic Nomenclature and Classification of Porosity in Sedimentary Carbonates." *American Association of Petroleum Geologists Bulletin* 54: 207–250.

Corsetti, F. A., and J. P. Grotzinger. 2005. "Origin and Significance of Tube Structures in Neoproterozoic Post-Glacial Cap Carbonates: Example From Noonday Dolomite, Death Valley, United States." *PALAIOS* 20: 348–362.

Costerton, J. W., Z. Lewandowski, D. DeBeer, D. Caldwell, D. Korber, and G. James. 1994. "Biofilms, the Customized Microniche." *Journal of Bacteriology* 176: 2137–2142.

Decho, A. W., P. T. Visscher, and R. P. Reid. 2005. "Production and Cycling of Natural Microbial Exopolymers (EPS) Within a Marine



Stromatolite." Palaeogeography, Palaeoclimatology, Palaeoecology 219: 71–86.

Dupraz, C., A. Fowler, C. Tobias, and P. T. Visscher. 2013. "Stromatolitic Knobs in Storr's Lake (San Salvador, Bahamas): A Model System for Formation and Alteration of Laminae." *Geobiology* 11: 527–548.

Dupraz, C., and P. T. Visscher. 2005. "Microbial Lithification in Marine Stromatolites and Hypersaline Mats." *Trends in Microbiology* 13: 429–438.

Ehrlich, H., J. K. Rigby, J. P. Botting, et al. 2013. "Discovery of 505-Million-Year Old Chitin in the Basal Demosponge Vauxia Gracilenta." *Scientific Reports* 3: 17–20.

Flemming, H. C., and J. Wingender. 2010. "The Biofilm Matrix." *Nature Reviews Microbiology* 8: 623–633.

Flügel, E. 2004. Microfacies of Carbonate Rocks: Analysis, Interpretation, and Application. New York, NY: Springer.

Fraiser, M. L., and F. A. Corsetti. 2003. "Neoproterozoic Carbonate Shrubs: Interplay of Microbial Activity and Unusual Environmental Conditions in Post-Snowball Earth Oceans." *PALAIOS* 18: 378–387.

Friesenbichler, E., S. Richoz, A. Baud, et al. 2018. "Sponge-Microbial Build-Ups From the Lowermost Triassic Chanakhchi Section in Southern Armenia: Microfacies and Stable Carbon Isotopes." *Palaeogeography, Palaeoclimatology, Palaeoecology* 490: 653–672.

Froget, C. 1976. "Observations Sur L'altération de la Silice et des Silicates au Cours de la Lithification Carbonatée (Région Siculo-Tunisienne)." *Géologie Méditerranéenne* 3: 219–225.

Geisel, S., E. Secchi, and J. Vermant. 2022. "The Role of Surface Adhesion on the Macroscopic Wrinkling of Biofilms." *eLife* 11: 1–19.

Grey, K., and S. M. Awramik. 2020. *Handbook for the Study and Description of Microbialites*, 147. Australia Bulletin: Geological Survey of Western Australia Bulletin.

Grotzinger, J. P., and A. H. Knoll. 1995. "Anomalous Carbonate Precipitates: Is the Precambrian the Key to the Permian?" *PALAIOS* 10: 578–596.

Gürich, G. J. E. 1906. Les Spongiostromides du Viséen de la Province de NAMUR. Mémoires du Musée Royal D'Histoire Naturelle de Belgique = Verhandelingen van het Koninklijk Natuurhistorisch Museum van Belgie. Musée Royal d'Histoire Naturelle de Belgique, Bruxelles: Imprimerie Polleunis & Ceuterick.

Hamilton, D. 1961. "Algal Growths in the Rhaetic Cotham Marble of Southern England." *Palaeontology* 4: 324–333.

Heindel, K., W. J. Foster, S. Richoz, et al. 2018. "The Formation of Microbial-Metazoan Bioherms and Biostromes Following the Latest Permian Mass Extinction." *Gondwana Research* 61: 187–202.

Hesselbo, S. P., S. A. Robinson, and F. Surlyk. 2004. "Sea-Level Change and Facies Development Across Potential Triassic–Jurassic Boundary Horizons, SW Britain." *Journal of the Geological Society* 161: 365–379.

Hopkins, M. J., and S. Gerber. 2017. "Morphological Disparity." In *Evolutionary Developmental Biology: A Reference Guide*, edited by L. Nuno de la Rosa and G. Müller, 1–12. Cham, Switzerland: Springer International Publishing.

Ibarra, Y., and F. A. Corsetti. 2016. "Lateral Comparative Investigation of Stromatolites: Astrobiological Implications and Assessment of Scales of Control." *Astrobiology* 16: 271–281.

Ibarra, Y., F. A. Corsetti, S. E. Greene, and D. J. Bottjer. 2014. "Microfacies of the Cotham Marble: A Tubestone Carbonate Microbialite From the Upper Triassic Southwestern U.K." *PALAIOS* 29: 1–15.

Ibarra, Y., F. A. Corsetti, S. E. Greene, and D. J. Bottjer. 2015. "Microfacies of the Cotham Marble: A Tubestone Carbonate Microbialite From the Upper Triassic Southwestern U.K.: A Reply." *PALAIOS* 30: 806–809.

Ibarra, Y., F. A. Corsetti, S. E. Greene, and D. J. Bottjer. 2016. "A Microbial Carbonate Response in Synchrony With the End-Triassic Mass Extinction Across the SW UK." *Scientific Reports* 6: 19808.

Jesionowski, T., M. Norman, S. Zółtowska-Aksamitowska, I. Petrenko, Y. Joseph, and H. Ehrlich. 2018. "Marine Spongin: Naturally Prefabricated 3D Scaffold-Based Biomaterial." *Marine Drugs* 16: 1–23.

Kershaw, S., Q. Li, and Y. Li. 2021. "Addressing a Phanerozoic Carbonate Facies Conundrum—Sponges or Clotted Micrite? Evidence From Early Silurian Reefs, South China Block." *Sedimentary Record* 19: 3–10.

Kropp, J., A. Block, B. W. Von, T. Klenke, and H. J. Schellnhuber. 1997. "Multifractal Characterization of Microbially Induced Magnesian Calcite Formation in Recent Tidal Flat Sediments." *Sedimentary Geology* 109: 37–51.

Lawrence, J. R., D. R. Korber, B. D. Hoyle, J. W. Costerton, and D. E. Caldwell. 1991. "Optical Sectioning of Microbial Biofilms." *Journal of Bacteriology* 173: 6558–6567.

Lee, J. H., J. Chen, S. J. Choh, D. J. Lee, Z. Han, and S. K. Chough. 2014. "Furongian (Late Cambrian) Sponge-Microbial Maze-Like Reefs in the North China Platform." *PALAIOS* 29: 27–37.

Lee, J. H., and R. Riding. 2021. "The 'Classic Stromatolite' Cryptozoön is a Keratose Sponge-Microbial Consortium." *Geobiology* 19: 189–198.

Lee, J.-H., and R. Riding. 2022. "Recognizing Sponge in Spongiostroma Gürich, 1906 From the Mississippian of Belgium." *Journal of Paleontology* 96: 1–12.

Lei, W., P. Krolla, T. Schwartz, and P. A. Levkin. 2020. "Controlling Geometry and Flow Through Bacterial Bridges on Patterned Lubricant-Infused Surfaces (pLIS)." *Small* 16: 1–7.

Luo, C., Y. Pei, S. Richoz, Q. Li, and J. Reitner. 2022. "Identification and Current Palaeobiological Understanding of "Keratosa"-Type Nonspicular Demosponge Fossils in Carbonates: With a New Example from the Lowermost Triassic, Armenia." *Life* 12: 1348.

Luo, C., and J. Reitner. 2014. "First Report of Fossil "Keratose" Demosponges in Phanerozoic Carbonates: Preservation and 3-D Reconstruction." *Naturwissenschaften* 101: 467–477.

Luo, C., and J. Reitner. 2016. "'Stromatolites' Built By Sponges and Microbes – A New Type of Phanerozoic Bioconstruction." *Lethaia* 49: 555–570.

Mackey, T. J., D. Y. Sumner, I. Hawes, et al. 2017. "Increased Mud Deposition Reduces Stromatolite Complexity." *Geology* 45: 663–666.

Marenco, P. J., F. A. Corsetti, and D. J. Bottjer. 2002. "Noonday Tubes: Observations and Reinterpretations Based on Better Preservation From a New Locality." In *Proterozoic-Cambrian of the Great Basin and Beyond, Pacific Section Book* (Vol 93), edited by F. Corsetti, 31–42. Fullerton, California: Pacific Section SEPM (Society for Sedimentary Geology).

Martinho De Brito, M., I. Bundeleva, F. Marin, et al. 2023. "Properties of Exopolymeric Substances (EPSs) Produced During Cyanobacterial Growth: Potential Role in Whiting Events." *Biogeosciences* 20: 3165–3183.

Mehra, A., W. A. Watters, J. P. Grotzinger, and A. C. Maloof. 2020. "Three-Dimensional Reconstructions of the Putative Metazoan Namapoikia Show That It Was a Microbial Construction." *Proceedings of the National Academy of Sciences of the United States of America* 117: 19760–19766.

Neuweiler, F., S. Kershaw, F. Boulvain, et al. 2023. "Keratose Sponges in Ancient Carbonates – A Problem of Interpretation." *Sedimentology* 70: 927–968.

Otsu, N. 1979. "A Threshold Selection Method From Gray-Level Histograms." *IEEE Transactions on Systems, Man, and Cybernetics* 9: 62–66.



Park, J., J. H. Lee, J. Hong, S. J. Choh, D. C. Lee, and D. J. Lee. 2015. "An Upper Ordovician Sponge-Bearing Micritic Limestone and Implication for Early Palaeozoic Carbonate Successions." *Sedimentary Geology* 319: 124–133.

Pei, Y., J. P. Duda, J. Schönig, C. Luo, and J. Reitner. 2021. "Late Anisian Microbe-Metazoan Build-Ups in the Germanic Basin: Aftermath of the Permian–Triassic Crisis." *Lethaia* 54: 823–844.

Penesyan, A., I. T. Paulsen, S. Kjelleberg, and M. R. Gillings. 2021. "Three Faces of Biofilms: A Microbial Lifestyle, a Nascent Multicellular Organism, and an Incubator for Diversity." *NPJ Biofilms and Microbiomes* 7: 1–9.

Petroff, A. P., M. S. Sim, A. Maslov, M. Krupenin, D. H. Rothman, and T. Bosak. 2010. "Biophysical Basis for the Geometry of Conical Stromatolites." *Proceedings of the National Academy of Sciences of the United States of America* 107: 9956–9961.

Petryshyn, V. A., S. E. Greene, A. Farnsworth, et al. 2020. "The Role of Temperature in the Initiation of the End-Triassic Mass Extinction." *Earth-Science Reviews* 208: 103266.

Pratt, B. R. 1982. "Stromatolitic Framework of Carbonate Mud-Mounds." *Journal of Sedimentary Petrology* 52: 1203–1227.

Quan, K., J. Hou, Z. Zhang, et al. 2022. "Water in Bacterial Biofilms: Pores and Channels, Storage and Transport Functions." *Critical Reviews in Microbiology* 48: 283–302.

Riding, R. 2002. "Biofilm Architecture of Phanerozoic Cryptic Carbonate Marine Veneers." *Geology* 30: 31–34.

Ritterbush, K. A., S. Rosas, F. A. Corsetti, D. J. Bottjer, and A. J. West. 2015. "Andean Sponges Reveal Long-Term Benthic Ecosystem Shifts Following the End-Triassic Mass Extinction." *Palaeogeography, Palaeoeclimatology, Palaeoecology* 420: 193–209.

Rooney, L. M., W. B. Amos, P. A. Hoskisson, and G. McConnell. 2020. "Intra-Colony Channels in *E. coli* Function as a Nutrient Uptake System." *ISME Journal* 14: 2461–2473.

Sepkoski, J. J. 1982. "Flat-Pebble Conglomerates, Storm Deposits, and the Cambrian Bottom Fauna." In *Cyclic and Event Stratification*, edited by G. Einsele and A. Seilacher, 371–385. Berlin Heidelberg, Germany: Springer.

Shapiro, R. S. 2000. "A Comment on the Systematic Confusion of Thrombolites." *PALAIOS* 15: 166–169.

Shepard, R. N., and D. Y. Sumner. 2010. "Undirected Motility of Filamentous Cyanobacteria Produces Reticulate Mats." *Geobiology* 8: 179–190.

Sim, M. S., B. Liang, A. P. Petroff, et al. 2012. "Oxygen-Dependent Morphogenesis of Modern Clumped Photosynthetic Mats and Implications for the Archean Stromatolite Record." *Geosciences* 2: 235–259.

Stewart, P. S. 2012. "Mini-Review: Convection Around Biofilms." *Biofouling* 28: 187–198.

Stocchino, G. A., T. Cubeddu, R. Pronzato, M. A. Sanna, and R. Manconi. 2021. "Sponges Architecture by Colour: New Insights Into the Fibres Morphogenesis, Skeletal Spatial Layout and Morpho-Anatomical Traits of a Marine Horny Sponge Species (Porifera)." *European Zoological Journal* 88: 237–253.

Stoodley, P., D. DeBeer, and Z. Lewandowski. 1994. "Liquid Flow in Biofilm Systems." *Applied and Environmental Microbiology* 60: 2711–2716

Taylor, M. W., R. Radax, D. Steger, and M. Wagner. 2007. "Sponge-Associated Microorganisms: Evolution, Ecology, and Biotechnological Potential." *Microbiology and Molecular Biology Reviews* 71: 295–347.

Tebbutt, G. E., C. D. Conley, and D. W. Boyd. 1965. "Lithogenesis of a Distinctive Carbonate Rock Fabric." *University of Wyoming Contributions to Geology* 4: 1–13.

Turner, E. C. 2021. "Possible Poriferan Body Fossils in Early Neoproterozoic Microbial Reefs." *Nature* 596: 87–91.

Walcott, C. D. 1920. Cambrian Geology and Paleontology. IV. Middle Cambrian Spongiae, 261–364. Washington D.C.: Smithsonian Institution. Smithsonian Miscellaneous Collections 67.

Walter, M. R. 1972. Stromatolites and the Biostratigraphy of the Australian Pre-Cambrian and Cambrian, 256. London: Palaeontological Association of London. Special Papers in Palaeontology, Vol. 11.

Wilking, J. N., V. Zaburdaev, V. M. De, R. Losick, M. P. Brenner, and D. A. Weitz. 2013. "Liquid Transport Facilitated by Channels in *Bacillus subtilis* Biofilms." *Proceedings of the National Academy of Sciences of the United States of America* 110: 848–852.

Woods, A. D., D. J. Bottjer, M. Mutti, and J. Morrison. 1999. "Lower Triassic Large Sea-Floor Carbonate Cements: Their Origin and a Mechanism for the Prolonged Biotic Recovery From the End-Permian Mass Extinction." *Geology* 27: 645–648.

Wright, V. P., and M. Mayall. 1981. "Organism-Sediment Interactions in Stromatolites: An Example From the Upper Triassic of South West Britain." Phanerozoic Stromatolites 74–84.

Wu, S., Z. Q. Chen, C. Su, Y. Fang, and H. Yang. 2022. "Keratose Sponge Fabrics From the Lowermost Triassic Microbialites in South China: Geobiologic Features and Phanerozoic Evolution." *Global and Planetary Change* 211: 103787.

Yan, J., A. G. Sharo, H. A. Stone, N. S. Wingreen, and B. L. Bassler. 2016. "Vibrio Cholerae Biofilm Growth Program and Architecture Revealed by Single-Cell Live Imaging." *Proceedings of the National Academy of Sciences of the United States of America* 113: e5337–e5343.

Zhang, N., C. E. L. Thompson, I. H. Townend, K. E. Rankin, D. M. Paterson, and A. J. Manning. 2018. "Nondestructive 3D Imaging and Quantification of Hydrated Biofilm-Sediment Aggregates Using X-Ray Microcomputed Tomography." *Environmental Science and Technology* 52: 13306–13313.

Supporting Information

Additional supporting information can be found online in the Supporting Information section.

